

Model-based Reconstruction for Real-Time Phase-Contrast Flow MRI - Improved Spatiotemporal Accuracy

Zhengguo Tan¹, Volkert Roeloffs¹, Dirk Voit¹, Arun Joseph¹, Markus Untenberger¹, Klaus-Dietmar Merboldt¹, and Jens Frahm¹¹Biomedizinische NMR Forschungs GmbH, Max-Planck-Institute for Biophysical Chemistry, Goettingen, Germany

Synopsis

The proposed model-based reconstruction technique jointly computes a magnitude image, a phase-contrast map, and a set of coil sensitivities from every pair of flow-compensated and flow-encoded datasets obtained by highly undersampled radial FLASH. Real-time acquisitions with 5 and 7 radial spokes per image resulted in 25.6 and 35.7 ms measuring time per phase-contrast map, respectively. It yields quantitatively accurate phase-contrast maps with improved spatial acuity, reduced phase noise, reduced partial volume effects, and reduced streaking artifacts.

Purpose

To develop a model-based reconstruction technique for real-time phase-contrast flow MRI with improved spatiotemporal accuracy in comparison to methods using phase differences of two separately reconstructed images with differential flow encodings.

Methods

The signal model assumes the same magnitude image and the same coil sensitivities for each pair of flow-compensated and flow-encoded datasets, and thus the forward model of the j^{th} coil in the l^{th} acquisition is $F_{j,l}(x) = P_l \cdot \mathcal{F}\{\rho \cdot e^{z \cdot S_l} \cdot c_j\}$, where ρ is the magnitude image, z denotes a complex map which contains the phase differences $\Delta\phi$ in the imaginary part, while its real part is constrained to be zero, c_j is the sensitivity map of the j^{th} coil. The indices $S_1 = 0$ and $S_2 = 1$ represent the flow-compensated and the flow-encoded acquisition, respectively. P_l is the orthogonal projection onto the l^{th} trajectory¹. The unknowns ρ , z , and c_j in this nonlinear signal model can be solved by the iteratively regularized Gauss-Newton method as introduced for nonlinear inversion (NLINV)¹. Moreover, a L2-norm regularization on z is used with the initial guess of zero, and the temporal regularization¹ is adopted on z as well. The partial derivatives and regularization among unknowns are balanced via an automatic scaling on S_l . The scaling value can be derived via the definition of the complex-difference (CD) image²: $CD = |\rho_1 - \rho_2| = M \cdot \sqrt{2[1 - \cos(\Delta\phi)]}$. It can be proven to hold that $\|\sqrt{2[1 - \cos(\Delta\phi)]}\|_2 \propto \|\Delta\phi\|_2$, and thus the scaled index is $\hat{S}_l = \|M\|_2 / \|CD\|_2$. M and CD can be calculated by the mean and complex-difference of the gridded multi-channel k-space data from the flow-compensated and the flow-encoded acquisition, respectively. In fact, based on the linearity of the Fourier transformation, the norm of an image is equivalent to that in k-space.

Real-time flow MRI was based on extremely undersampled radial FLASH (5 or 7 spokes per image) using two sequential acquisitions of a dataset with velocity-compensated gradients in all gradient axes and with velocity-encoding of through-plane flow, respectively. All measurements (TE = 1.70 ms, flip angle 10 degree) had 1.5 mm in-plane resolution, 320 mm field-of-view, 6 mm slice thickness, and 35.7 ms (7 spokes, TR = 2.55 ms) or 25.6 ms (5 spokes, TR = 2.56 ms) temporal resolution corresponding to 28 or 39 frames per second, respectively. This work presents real-time flow MRI of the aorta acquired from 10 healthy subjects and 2 patients with combined aortic valve insufficiency and partial stenosis³.

Results & Discussion

Qualitative comparisons of NLINV and model-based phase-contrast MRI are depicted in Fig. 1 for a normal subject and in Fig. 2 for a patient with aortic valve insufficiency and partial stenosis, respectively. The systolic phase-contrast maps obtained by the model-based reconstruction yield a much better spatial definition in regions with non-zero flow (i.e., vessels). Here, this particularly applies to the descending aorta whose phase-difference presentation is in close agreement with the vessel lumen in the magnitude image. In addition, the implicit a priori knowledge of zero phase in pixels without flowing spins precludes the iterative optimization process to generate residual streaking artifacts in areas around vessels with maximum systolic flow, i.e. for signals with high temporal and spatial frequencies that are most severely affected by k-space undersampling. Moreover, as shown in the phase-contrast map from NLINV in Fig. 2, the pixels in the top-left border of the ascending aorta suffer from partial volume effects. This is unavoidable in the phase-difference reconstruction²

when both stationary and flowing magnetizations are present within a single voxel, and usually appears for patients with thicker vessels. However, because of improved spatial acuity, such problems are largely avoided in the model-based reconstruction.

The spatiotemporal improvement achievable by model-based phase-contrast flow MRI may be invested into even faster acquisitions. Fig. 3 advances real-time phase-contrast flow MRI from 7 spokes per image and 35.7 ms total acquisition time to 5 spokes and 25.6 ms temporal resolution. This clearly supports the notion that the use of 5 spokes represents an extreme but feasible approach to real-time flow MRI.

Quantitative results are summarized in Tables 1³ and 2 (new healthy volunteers) and found to be in general agreement.

Conclusion

Under all conditions, and compared to a previously developed real-time flow MRI method, the proposed method yields quantitatively accurate phase-contrast maps (i.e. flow velocities) with improved spatial acuity, reduced phase noise, reduced partial volume effects, and reduced streaking artifacts. This novel model-based reconstruction technique may become a new tool for clinical flow MRI in real time.

Acknowledgements

The authors thank Drs. Anja Hennemuth, Teodora Chitiboi, and Markus Hüllebrandt of the Fraunhofer MEVIS Institute for Medical Image Computing, Bremen, Germany, for developing specialized CAIPI software for real-time MRI. We also thank Prof. Dr. Christina Unterberg-Buchwald of the Clinic for Cardiology and Pneumology, University Medical Center Göttingen, Germany, for letting us study her patients. Finally, we are grateful to Dr. Oleksandr Kalentev for numerous discussions and Christian Holme for help with Compute Unified Device Architecture (CUDA) C programming.

References

1. Uecker M, Hohage T, Block KT, et al. Image reconstruction by regularized nonlinear inversion - Joint estimation of coil sensitivities and image content. *Mag Reson Med* 2008;60:674-682.
2. Bernstein MA, King FK, Zhou XJ. *Handbook of MRI pulse sequences*. Burlington, MA: Elsevier Academic Press; 2004.
3. Untenberger M, Tan Z, Voit D, et al. Advances in real-time phase-contrast flow MRI using asymmetric radial gradient echoes. *Magn Reson Med* 2015; doi: 10.1002/mrm.25696.

Figures

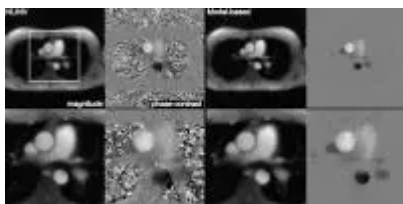


Fig. 1. Systolic magnitude images and phase-contrast maps via (left) NLINV and model-based reconstructions for real-time phase-contrast MRI of aortic blood flow (35.7 ms resolution, VENC = 200 cm s⁻¹) in a healthy volunteer. The lower panels represent magnified views.

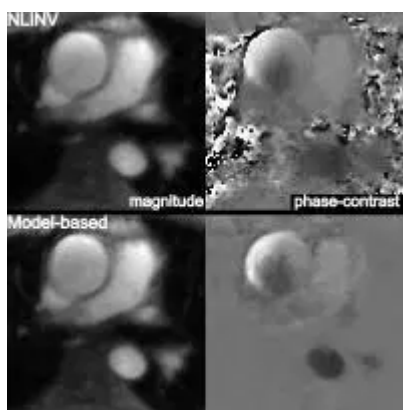


Fig. 2. (Top) NLINV and (bottom) model-based reconstructions of systolic magnitude images and phase-contrast maps (magnified views) for real-time phase-contrast MRI of aortic blood flow (35.7 ms resolution, VENC=400 cm s⁻¹) in a patient with aortic valve insufficiency and partial stenosis.

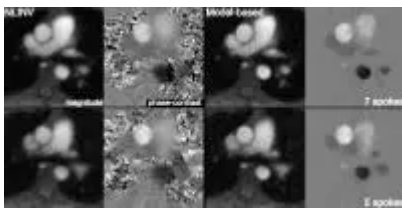


Fig. 3. (Left) NLIIV and (right) model-based reconstructions of systolic magnitude images and phase-contrast maps (magnified views) for real-time phase-contrast MRI of aortic blood flow (VENC = 200 cm s⁻¹) in a healthy volunteer using (top) 7 spokes per frame at 35.7 ms resolution and (bottom) 5 spokes per frame at 25.6 ms resolution.

Subject	Reconstruction Technique	Peak Velocity cm s ⁻¹	Flow per HeartBeat mL	Flow Volume L	Reconstruction Fraction %
#1	NLIIV	128 ± 3	89 ± 4	5.7 ± 0.4	2 ± 1
	Model-based	121 ± 4	81 ± 5	5.2 ± 0.5	7 ± 1
#2	NLIIV	114 ± 8	128 ± 8	6.8 ± 0.3	7 ± 1
	Model-based	114 ± 7	112 ± 5	6.3 ± 0.2	7 ± 1
#3	NLIIV	69 ± 3	61 ± 3	4.0 ± 0.2	2 ± 1
	Model-based	39 ± 4	62 ± 2	4.1 ± 0.2	7 ± 1
#4	NLIIV	112 ± 8	121 ± 4	6.1 ± 0.3	2 ± 1
	Model-based	111 ± 4	123 ± 4	7.8 ± 0.3	2 ± 1
#5	NLIIV	100 ± 3	107 ± 3	6.3 ± 0.1	3 ± 1
	Model-based	108 ± 5	87 ± 3	5.6 ± 0.1	4 ± 1
Pat #1	NLIIV	264 ± 14	66 ± 8	3.8 ± 0.3	35 ± 3
	Model-based	218 ± 11	81 ± 5	2.8 ± 0.2	37 ± 2
Pat #2	NLIIV	202 ± 10	82 ± 9	5.3 ± 0.3	18 ± 2
	Model-based	219 ± 6	71 ± 6	4.6 ± 0.4	23 ± 3

Table 1. Quantitative flow evaluations of the ascending aorta of 5 healthy volunteers and 2 patients with valve insufficiency (data from Ref. [2])

Subject	Spokes per image	Ascending Aorta		Descending Aorta	
		Peak Velocity cm s ⁻¹	Flow per HeartBeat mL	Peak Velocity cm s ⁻¹	Flow per HeartBeat mL
#6	7	88 ± 4	88 ± 9	88 ± 5	80 ± 5
	5	88 ± 4	100 ± 4	101 ± 5	170 ± 3
#7	7	127 ± 8	107 ± 6	128 ± 5	81 ± 4
	5	126 ± 8	84 ± 5	125 ± 8	86 ± 4
#8	7	83 ± 7	77 ± 7	104 ± 8	52 ± 4
	5	84 ± 10	78 ± 7	104 ± 8	56 ± 4
#9	7	134 ± 3	106 ± 4	139 ± 3	66 ± 3
	5	116 ± 2	103 ± 5	135 ± 3	65 ± 4
#10	7	88 ± 5	81 ± 3	180 ± 5	54 ± 3
	5	86 ± 3	75 ± 4	180 ± 3	54 ± 3

Table 2. Quantitative flow evaluations of model-based reconstructions in the ascending and descending aorta of healthy volunteers